Field-induced self-assembled ferrofluid aggregation in pulsatile flow

Ranjan Ganguly, Brian Zellmer, and Ishwar K. Puri

Citation: Physics of Fluids (1994-present) **17**, 097104 (2005); doi: 10.1063/1.2040307
View online: http://dx.doi.org/10.1063/1.2040307
View Table of Contents: http://scitation.aip.org/content/aip/journal/pof2/17/9?ver=pdfcov
Published by the AIP Publishing

Field-induced self-assembled ferrofluid aggregation in pulsatile flow

Ranjan Ganguly,[a),b)] Brian Zellmer,[b)] and Ishwar K. Puri[c)]
Department of Engineering Science and Mechanics, Virginia Polytechnic Institute and State University, Blacksburg, Virginia 24061

(Received 27 May 2005; accepted 26 July 2005; published online 2 September 2005)

Ferrofluid aggregation and dispersion occurs at several length scales in pulsatile flow applications, e.g., in ferrofluidic pumps, valves, and biomedical applications such as magnetic drug targeting. Because of a yet limited understanding, ferrohydrodynamic investigations involving laboratory-scale studies in idealized geometries are of considerable use. We have injected a ferrofluid into a pulsatile host flow and produced field-induced dissolution (aggregation) using external magnets. A comparison is made with ferrofluid aggregation in a steady flow. Subsequently, the accumulation and dispersion of the ferrofluid aggregates in pulsatile flow are characterized by analyzing their size, mean position, and the flow frequency spectrum. The maximum aggregate size A_{max}, time to form it t_{max}, and the aggregate half-life t_{half} are found to scale according to the relations $A_{max} \propto \mathrm{Re}^{-0.71}$, $t_{max} \propto \mathrm{Re}^{-2.1}$, and $t_{half} \propto \mathrm{Re}^{-2.2}$. While the experiments are conducted at a macroscopic length scale for useful experimental resolution, the results also enable an understanding of the micro- and mesoscale field-assisted self-assembly of magnetic nanoparticles. © *2005 American Institute of Physics*. [DOI: 10.1063/1.2040307]

I. INTRODUCTION

Ferrofluids are colloidal suspensions of single-domain magnetic nanoparticles containing Ni, Co, Mg, or Zn compositions of ferrite ($-Fe_2O_4$), magnetite (Fe_3O_4), and maghemite (γ-Fe_2O_3).[1,2] At normal temperatures ($\sim$300 K) the thermal Brownian energy of the individual particle magnetic domains is much larger than the magnetocrystalline anisotropy energy. Since the particles are generally 10-15 nm in diameter, the blocking temperature[3] is much lower than room temperature and hence the particles exhibit superparamagnetic behavior.[4] The individual particle dipoles are randomly oriented due to thermal agitation. Therefore, ferrofluids do not exhibit permanent magnetization, but demonstrate magnetic behavior only when an external magnetic field is imposed, which induces the alignment of the thermally disoriented magnetic moments of the nanoparticles. The nanoparticles are coated with adsorbed surfactant layers to prevent their agglomeration that would otherwise occur due to the attractive van der Waals forces and dipole-dipole interactions between them. The particles can also be "functionalized," i.e., they can be coated with suitable inorganic or organic molecules that serve specific chemical or biological tasks.[5]

Ferrofluids undergo magnetic field-assisted self-assembly to create two- or three-dimensional structures.[6–8] This assembly can be implemented at different length scales for various applications involving fluid flows, e.g., microfabrication, ferrofluid-based switches and valves, and magnetic drug targeting. For instance, a ferrofluid can be mixed with wet etching chemicals, subsequently introduced into narrow channels (where masking is otherwise difficult), and thereafter deposited on a substrate locally and selectively by imposing a suitably designed magnetic field. Thus, maskless etching of micro- or mesoscale channels can be accomplished by building ferrofluid aggregates on well-defined targets. Three-dimensional ferrofluid aggregates can also be used as microfluidic components in pumps and valves[9] or as microsize contact switches. In a ferrofluid micropump, a magnetic field-driven ferrofluid droplet acts as a reciprocating piston in a microchannel to pump another fluid. With microvalves, similar aggregates (again produced by imposing a magnetic field) are used to enable or prevent the flow in microchannels. In ferrofluid microcontact switches, liquid bridges of electrically conductive ferrofluids are produced under the influence of a magnetic field to establish contacts between two electrodes that are immersed in an immiscible fluid. All these applications rely on proper ferrofluid aggregation by imposing a magnetic field. For the devices to work, it is important that the ferrofluid structures maintain their integrity against the shear force exerted in either a steady or periodic flow.

Similar self-assembled aggregates must be produced for a number of biomedical applications such as magnetic drug targeting (MDT),[10,11] magnetic fluid hyperthermia,[12] and magnetic resonance imaging (MRI) contrast enhancement.[13] MDT is a promising technique for the treatment of various diseases and cardiovascular episodes such as stenosis and thrombosis.[10] Here, magnetically guided aggregates of a biocompatible ferrofluid that have specific chemotherapeutic agents bonded to the superparamagnetic nanoparticles are injected into the blood or lymphatic circulation system. The aggregates carry medicinal drugs and release them at target sites in the human body. Similar *in vivo* targeting of magnetic nanoparticles through the pulsatile flow in the human

[a)]Present address: Power Engineering Department, Jadavpur University, Kolkata, 700032, India.
[b)]Present address: Department of Mechanical and Industrial Engineering, University of Illinois at Chicago, IL 60607.
[c)]Author to whom correspondence should be addressed; electronic mail: ikpuri@vt.edu

circulation system can be applied for induced hyperthermia and enhanced MRI applications. Since the US Federal Drug Administration (FDA)-approved human exposure limit to static magnetic fields is relatively high (e.g., 2 T for the entire body and 5 T for a limb), fairly large magnetic field gradients can be used without detrimental side effects. Again, for these applications, the magnetic nanoparticles are influenced by magnetic fields generated outside the human body that produce the desired transport characteristics.[14]

While the physical principles underlying the design of the magnetic manipulation devices are challenging, a proper understanding of ferrohydrodynamics and particle transport and dispersion is a necessary first step to localize the ferrofluid nanoparticles at a target location. In particular, the retention time of an aggregate of appropriate size and concentration before it is washed away from a targeted location (e.g., by a pulsatile blood flow, or by the buffer fluid in a microchannel) is an important parameter to characterize sufficient functional activity of the nanoparticles (e.g., drug desorption in case of MDT or the action of chemical etching in case of microfabrication). The literature in this regard is not at all well developed.

Although there have been a few previous investigations of the dispersion of soluble particles injected into steady or pulsating flows,[15,16] none of these have considered the presence of a magnetic body force on the particles. Voltairas *et al.*[17] presented a phenomenological description of a hemispherical magnetic fluid droplet in a Poiseuille flow adhering to the wall of a blood vessel that had a diameter much larger than of the droplet. However, they neglected to consider ferrofluid diffusion and dispersion into the host flow and its pulsations. In a similar experiment, Ruuge and Rusetski[18] assessed the influence of various factors, such as flow volume, velocity, tube diameter, and ferrofluid viscosity that counter the magnetic restraint on a ferrofluid drop that is held stationary on a tube wall and contained in a nonmagnetic fluid flow. They observed for their experiments that the ferrofluid drop mass decreased according to an exponential function, implying that the drug release rate is not constant and also decreases over time. Chen and Liao[19] numerically analyzed the displacement of a miscible magnetic fluid layer in a capillary tube under the influence of a moving ring-shaped magnet. They found that in Stokes flow the diffusive spread of the ferrofluid decreases as the magnetic field strength is increased. However, they did not characterize ferrofluid aggregation due to self-assembly in a forced flow.

Recently, Ganguly *et al.*[20,21] characterized the complex hydrodynamic and magnetic force interactions on the dispersion of a magnetic fluid held in a steady Poiseuille flow. They enabled the field-assisted self-assembly of ferrofluid aggregates in a steady flow and produced solid structures, creating a tightly bound upstream "core" and a downstream dispersive "washaway" region. Herein, we extend that investigation to pulsatile flows. Again, a known ferrofluid volume is introduced into a forced flow and then localized by using an external magnet. Since the magnetic field gradient produces a discernable ferrofluid accumulation, we call this process a field-induced aggregation. However, this should not be confused with the phenomenon of agglomeration (which generally occurs when the colloidal stability of a ferrofluid breaks down due to strong interparticle dipole interaction and forms clusters).

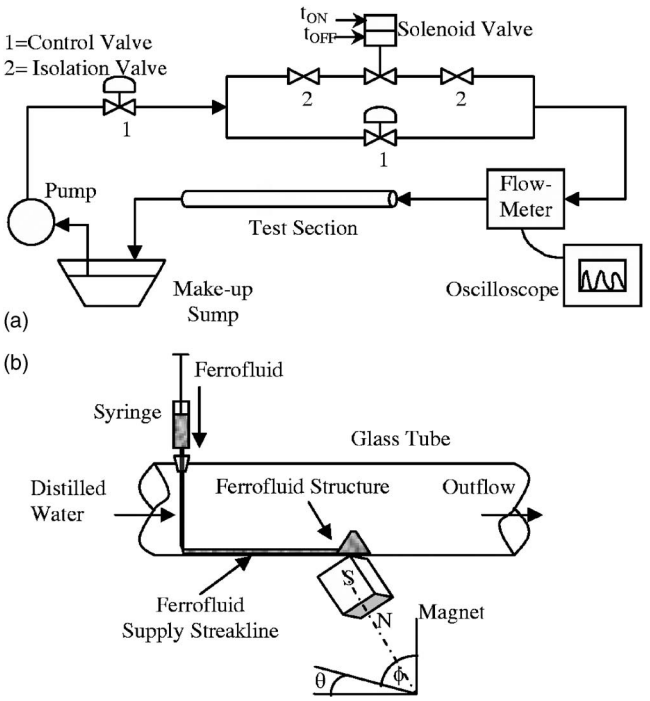

FIG. 1. Schematic arrangement of the experiment: (a) flow circuit and (b) enlarged view of the test section.

Ferrofluid dispersion is subsequently investigated by analyzing the aggregate size, mean position, and frequency spectrum. First, a comparison is made between the aggregation and dispersion in steady and pulsatile flows. The dependence of the dispersion rates on the mean flow Reynolds numbers for pulsatile flows is examined to develop a generalized relationship (that can be used for pulsatile flow applications, e.g., ferrofluid pumps or valves, or for *in vitro* MDT investigations). Our investigation is conducted at a macroscopic length scale for useful experimental resolution. This scale relates directly to large and medium blood vessels (arteries and veins) where the pressure has strong influence on the hydrodynamics. The basic understanding can be extended to miniaturized flow devices, since the results also enable an understanding of the micro- and mesoscale field-assisted self-assembly of magnetic nanoparticles.

II. EXPERIMENTAL METHOD

Figure 1 presents a schematic diagram of our experimental setup in which the three-dimensional ferrofluid structures are built. A known volume of EMG 705-series (FerroTec USA, NH) water soluble ferrofluid is released from a microliter syringe pump into a steady or pulsating laminar pipe flow of distilled water through a horizontally mounted glass tube (inner diameter 10 mm, length 1 m). The ferrofluid consists of a maximum of 4% by volume of magnetite that is dispersed uniformly in water by a water-soluble surfactant. It has a maximum specific gravity of 1.26, viscosity of 5 mPa s, and a saturation magnetization of 22 mT at 300 K.

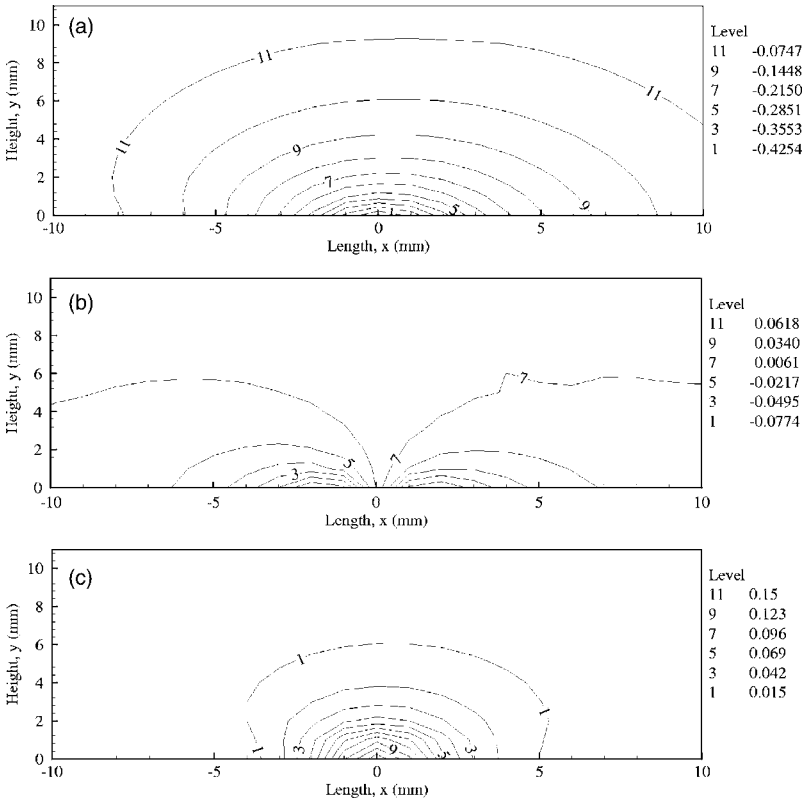

FIG. 2. Spatial variation of (a) the vertical component of the magnetic field B_y, and its gradients (b) $\partial B_y/\partial x$ and (c) $\partial B_y/\partial y$ along the vertical plane passing through the tube centerline. The location $y=0$ denotes the outer edge of the glass tube wall (of 1 mm thickness) and $x=0$ indicates the point where the bar magnet touches the wall (cf. Fig. 1). The magnetic field is represented in units of Tesla (T), while gradients are expressed as T/mm.

The injection volume is precisely measured from the syringe pump readings. Pulsation over a base flow rate in the test section is achieved though solenoid and control valves that are connected in parallel as shown in Fig. 1. The frequency and wave form of the flow can be adjusted by suitably regulating the "on" and "off" times of the solenoid valve, and the control valve. The flow circuit is operated in a semiopen cycle with a pump and a makeup sump. This provides flexibility in replacing the host fluid after repeated experiments once the dissolved ferrofluid concentration exceeds 5 ppm. A digital flow meter and an oscilloscope record the average flow rate and the pulsating flow wave form.

A syringe needle enters the tube vertically through a rubber plug and reaches the tube bottom as shown in Fig. 1. A rare-earth sintered NdFeB permanent magnet (2.54 cm $\times$2.54 cm$\times$2.54 cm) of 1.33 T remnant magnetism is placed under the tube 0.1 m downstream of the injection location to establish the magnetic field. The position and angular orientation of the magnet can be altered, since it is mounted on a graduated arc slider with two degrees of rotation and is also capable of moving perpendicular to the tube. Here, the magnet was mounted at $\theta=\phi=45°$ with one corner of its pole face touching the lower edge of the glass tube. Positioning of the magnet in such a manner produces the largest possible gradient in the magnetic field at the test section and thus maximizes the magnetic body force.

The spatial distribution of the magnetic field was measured with a 0.5 mm resolution using a Gaussmeter that had its probe mounted on a traversing mechanism. The vertical component of the resulting magnetic field and its gradients are shown in Fig. 2. As seen from Fig. 2(a), the field intensity $|B_y|$ decreases rapidly from 0.42 T at $(x,y=0,0)$ to 0.2 T at $(x,y=0,2$ mm). The corresponding field gradients also have large values near the dipole, but diminish quickly moving away from it. The magnitudes of the field gradient components provide an indication of the magnetic body force that the ferrofluid experiences. It is clear from Fig. 2 that if the ferrofluid is present in sufficient concentration in the proximity of the dipole, it experiences a strong magnetic body force that rapidly diminishes in magnitude at farther locations. The dispersion and localization of the ferrofluid are observed from direct light extinction images that are acquired using a charge-coupled device (CCD) camera against a white backlight, since the ferrofluid is dark and opaque.

III. RESULTS AND DISCUSSION

Ferrofluid dispersion in a steady flow is first investigated for the purpose of comparison. A 3 μl ferrofluid volume is injected at a rate of $\sim$1 μl/s into a steady, fully developed pipe flow established at Re=382. Assuming an average particle diameter of $\sim$10 nm and applying the Stokes approximation, the ferrofluid diffusivity in distilled water is $\sim 10^{-11}$ m^2/s.[22] Therefore, the injected ferrofluid experiences very little cross-stream dispersion after leaving the injector tip. Since it is denser than distilled water, it is advected downstream as a narrow streakline along the lowermost tube section. The ferrofluid experiences a Kelvin body force [expressed per unit volume as $\mathfrak{I}_i=M_j(\partial B_j/\partial x_i)$;[23] here M denotes the ferrofluid magnetization per unit volume and B the magnetic field] when the spatially varying magnetic field (cf. Fig. 2) is imposed. This force is oriented in the direction of increasing field gradient. The ferrofluid is strongly attracted towards the dipole in the region immediately around it to

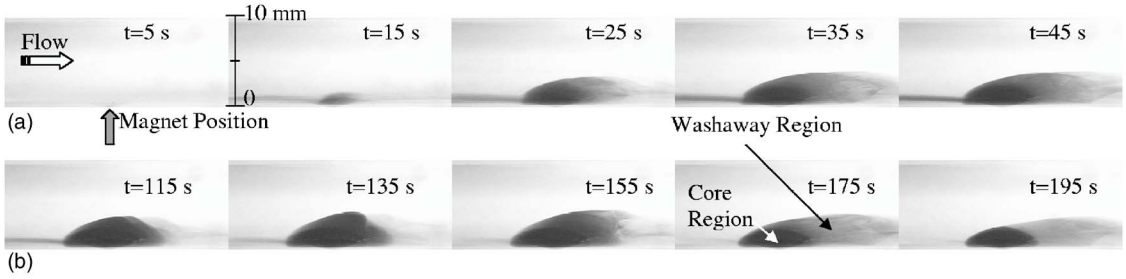

FIG. 3. Self-assembled ferrofluid accumulation and dispersion in a steady flow (Re=382). (a) The accumulation phase, and (b) the first washaway cycle following the accumulation phase.

form a hemispherical "core region." Ganguly *et al.*[21] have shown that this region behaves as a solid obstruction and creates a wake behind it.

The Kelvin body force is much less significant outside the core, since both the imposed magnetic field gradient and the local particle volume fraction are substantially smaller there. At some critical distance from the dipole, the magnetic body force becomes comparable to the fluid shear force. Therefore, ferrofluid advection occurs from the periphery of the core and forms a region of moderate concentration around it, which we call the washaway region.

Initially, following injection, ferrofluid accumulation occurs near the dipole, since the freshly supply exceeds its downstream dispersion. This buildup phase is shown in Fig. 3(a) during which the ferrofluid aggregate grows near the dipole. The pixel intensities in an image can be processed to determine the relative size of the projected area of the ferrofluid aggregate. Figure 4 presents the evolution of the projected areas thus determined in terms of the integrated pixel intensities for two flows, one steady and the other pulsatile. For both cases there is a 3 μl injected volume and the mean flow Re=382.

For the steady flow, accumulation occurs during the first 50 s. After fresh ferrofluid supply ceases, the mean aggregate size decreases due to its dispersion. Although the water (host) flow is steady and the magnetic field remains time invariant, ferrofluid dispersion occurs in cycles in accord with our previous finding.[21] Figure 4 shows the presence of four washaway cycles at ~155 s intervals before the aggregate amount reduces to less than 20% of its peak size after ~600 s. The periodic washaway behavior occurs due to instabilities that are produced through the interactions of the steady flow with (1) the solid core that behaves as an obstacle and (2) the magnetic field. Although the ferrofluid core is tightly held together by the magnetic field (due to both a high ferrofluid concentration and a large magnetic field gradient), the particles diffuse outward slowly because of the ferrofluid concentration gradient along the periphery of the core. In the peripheral region (where the both the ferrofluid concentration and the magnetic field gradient are not as high as in the core) the magnetic body force becomes weaker and is comparable to the fluid shear force. Here, flow perturbations influence the balance between the shear force (that seeks to disperse the particles) and the magnetic force (that attempts to retain these particles adjacent to the dipole). This produces an instability that leads to the periodic washaway.[21] It is apparent from Fig. 3(b) that the ferrofluid is dispersed from the core and spreads over a large area during each washaway cycle, and is eventually transported downstream, so that both the core and washaway regions eventually shrink. The integrated pixel intensity for the core has a half-life of 332 s, since the peak pixel density of 22.32 arbitrary units (a.u.) at $t=45$ s (the end of the accumulation phase) decreases to 11.16 a.u. at $t=332$ s.

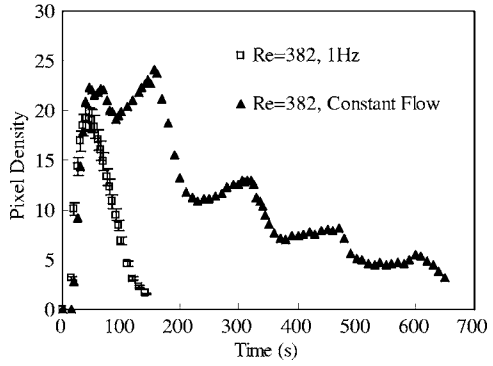

FIG. 4. Ferrofluid washaway profile for a steady flow and for a 1 Hz pulsatile flow (Re=382 for both). The pixel density (in arbitrary units) characterizes the ferrofluid accumulation at the target location in a qualitative manner.

In a 1 Hz frequency pulsatile flow (of mean Re=382), an accumulation phase followed by washaway is again observed for the ferrofluid aggregate. However, washaway occurs four times faster than for the steady flow as shown in Fig. 4 and, unlike for the steady flow, this washaway behavior is not periodic. The ferrofluid aggregate reaches its maximum size at $t=40$ s and the aggregate half-life is ~90 s. In Fig. 4, the pertinent curve is presented after averaging out ripples (represented by the vertical bars) for each 1 s period.

Figure 5 illustrates the oscillation of the ferrofluid aggregate during a complete 1 Hz flow cycle by presenting a sequence of images taken at 0.1 s intervals. The oscillations of the centroid of the projected areas of sequential aggregates (including the core and washaway regions) with respect to time are presented in Fig. 6. At $t=t_0$ (chosen arbitrarily at 56.1 s and corresponding to an early stage during the washaway phase), the instantaneous flow velocity is at a minimum and the periodic pressure gradient has its largest positive value (i.e., the pressure increases in the flow direction). Due to the positive pressure gradient at this instant, the centroid of the ferrofluid aggregate moves 1.3 mm upstream of the

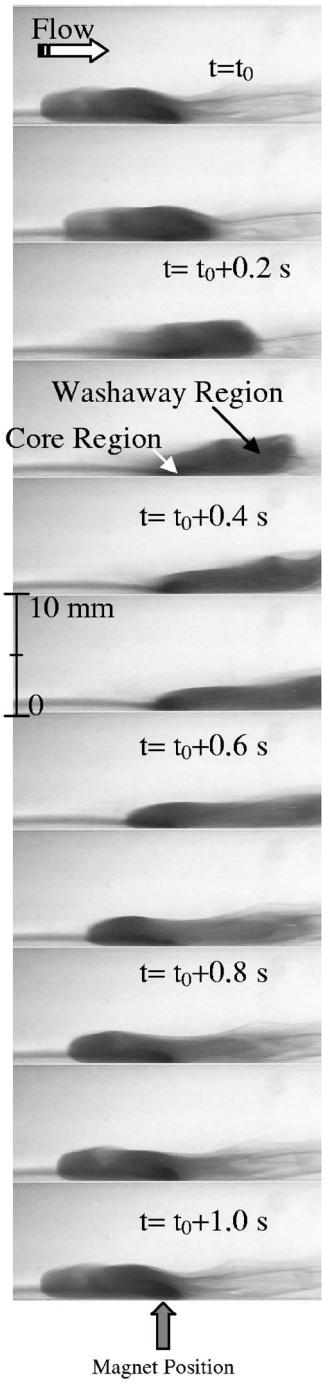

FIG. 5. The oscillation of a self-assembled ferrofluid aggregate during a single 1 Hz pulsating flow cycle (Re=382). Images represent the ferrofluid dispersion at 0.1 s intervals. t_0 corresponds to 56.1 s of Fig. 6.

dipole location (i.e., to $x=-1.3$ mm). As the cycle progresses, the pressure gradient becomes favorable (i.e., it becomes negative) in the flow direction and the aggregate now moves downstream. When the largest instantaneous flow occurs, the centroid shifts 4.5 mm downstream of the dipole (i.e., to $x=+4.5$ mm).

Figure 5 shows that the periodic flow alters the position, size, and shape of only the washaway region. Since the core is tightly held by the strong magnetic body force, it experiences relatively small oscillations in its location. During each

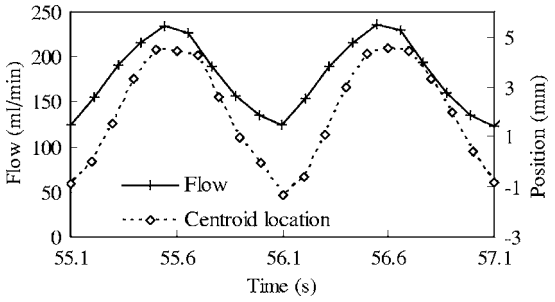

FIG. 6. Oscillation of the ferrofluid aggregate centroid (based on the pixel value) about the dipole location in one cycle of pulsating flow (1 Hz). The centroid shift closely follows the flow pulsation.

flow cycle the washaway region is swept downstream at the instants of maximum flow and retracts upstream as the flow subsides. The magnetic body force at downstream locations is weaker than that in the vicinity of the dipole so that a portion of the ferrofluid is able to escape downstream during each cycle. Hence, as shown in Fig. 4, the ferrofluid aggregate rapidly shrinks in comparison to its steady flow counterpart.

When the instantaneous integrated pixel intensity is plotted against time in Fig. 7 periodicity is also observed in the projected size of the aggregate. The ferrofluid aggregate shrinks when the pressure gradient is positive, but its response slightly lags the change in flow conditions. The ferrofluid mass increases when a favorable pressure gradient is present but the wave-form shape has higher frequency ripples. For the wave form of Fig. 7, the ferrofluid aggregate area fluctuates by $\sim 10\%$ about its mean, but the mean projected area decreases by only about 1% over a cycle. This fluctuation is further analyzed through its fast Fourier transformation (FFT). As can be seen from Figs. 6 and 7, the pulsatile flow had a fluctuating component of the order of 113 ml/min (i.e., the instantaneous flow varied between 238 and 125 ml/min) around a mean of 180 ml/min. This implies that the instantaneous Re oscillated from 505 to 265 about a mean of 382. The ripple factor $[=\sqrt{(\text{RMS value/mean value})^2-1}]$ for this wave form is 21.5%. The FFT of the flow presented in Fig. 8(a) shows a

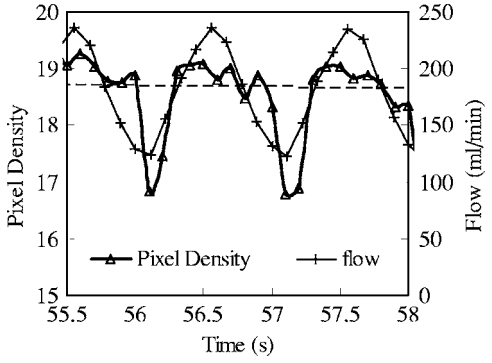

FIG. 7. Pulsation in the projected area of the ferrofluid aggregate (measured in terms of the variation of integrated pixel density in arbitrary units) with respect to time. The instantaneous flowmeter reading (ml/min) is superposed to show the phase relationship between the flow and ferrofluid dispersion. The dotted horizontal line represents the mean flow (180 ml/min).

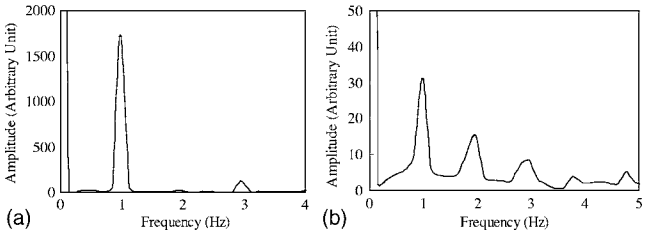

FIG. 8. FFT response of (a) the pulsatile flow rate, and (b) the pixel density profiles presented in Fig. 4. FFT of the flow profile shows a strong presence of the 1 Hz imposed frequency along with a higher harmonic at 3 Hz. Oscillation in the pixel density profile shows peak at 1, 2, 3, 3.8, and 4.8 Hz. Both the FFT results show high dc (zero frequency) components.

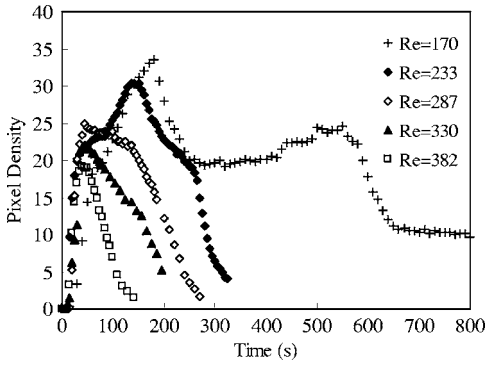

FIG. 9. Ferrofluid washaway profile for 1 Hz pulsatile flows established for different mean Re values. The pixel density (in arbitrary units) characterizes the ferrofluid accumulation at the target location in a qualitative manner.

strong component at 1 Hz as anticipated, which is followed by a weak component at ~3 Hz (with an amplitude is 7.3% of that at 1 Hz). The corresponding FFT of the integrated pixel intensities of the core regions is shown in Fig. 8(b). It has peaks at 1, ~2, ~3, ~3.8, and ~4.8 Hz. The relative magnitudes of the latter four peaks are respectively 49%, 27%, 13%, and 17% of the amplitude at 1 Hz. Both the flow and the pixel intensity FFTs show large dc (i.e., zero frequency) components that arise since both mean values are large compared to the corresponding fluctuations. The peaks at 1 Hz arise due to the flow pulsation. The flow wave form shown in Figs. 6 and 7 is not purely sinusoidal due to the behavior of the solenoid valves. Hence, a third harmonic is observed in both Figs. 8(a) and 8(b). However, the relative magnitude of this harmonic in case of the pixel intensity is much larger than for the flow wave form. There are other peaks at 2, 3.8, and 4.8 Hz that did not originate from the flow.

The magnetic body force is proportional to the local magnetic field gradient and the fluid magnetization. The fluid magnetization is obtained from Langevin equation, i.e., $M=\varphi M^{\mathrm{sat}}[\coth(\alpha)-(1/\alpha)]$, where φ is the volume fraction of magnetic particles in the fluid, M^{sat} is the bulk saturation magnetization of the particle material, and α is the Langevin parameter[21] (which is proportional to the magnetic field). Thus, in a nonuniform magnetic field (as described in Fig. 2), the Kelvin body force is highly nonlinear. On the other hand, the pulsatile flow can be approximated by the Womersley profile,[24] $v_z(\zeta,t)=\Sigma_{f=1,3}P_f a^2/i\rho\nu\mathrm{Wo}[1-J_0(i^{3/2}\mathrm{Wo}\zeta)/J_0(i^{3/2}\mathrm{Wo})]e^{i2\pi ft}$, where $i=\sqrt{-1}$, $v_z(\zeta,t)$ is the axial velocity profile, P_f is the amplitude of pressure pulses (corresponding to a frequency f) that drives the periodic flow, a is the pipe radius, ζ is the nondimensional radial position, $\mathrm{Wo}=a\sqrt{2\pi f/\nu}$ is the Womersley number, and ν and ρ are the kinematic viscosity and density of host fluid, respectively. The resulting shear force also possesses strong spatial nonlinearity. Since the ferrofluid aggregate size is influenced by interaction of magnetic force and shear force its transient behavior is also expected to show nonlinearity. Hence, it is expected that a comparison of the frequency spectra of the oscillation of pixel intensity data and the imposed flow pulsation would not show a one-to-one correspondence.

To determine the effect of the mean flow on the ferrofluid dispersion rate the integrated pixel intensities for the aggregates are plotted in Fig. 9 with respect to time for five 1 Hz pulsatile flows with mean Re values of 170, 233, 287, 330, and 382. For all flow conditions, the mean flow was changed, but the ripple factor values were kept within ±2.5% of the base value (which was 21.5%) by suitably adjusting the control valves 1 and 2 (refer to Fig. 1). All these flows corresponded to a Womersley number of 12.5. Again, for clarity, the ripples during each 1 s cycle are omitted in Fig. 9. In all cases, the ferrofluid aggregate first grows until the entire injected volume reaches the core location near the dipole. The smaller the value of Re, the less the initial transport rate towards the dipole and, consequently, the longer it takes to reach a maximum aggregate size. Although the washaway cycles observed for steady flow at Re=382 are absent from the corresponding (i.e., at the same Re) pulsatile flow, they reappear for the lower Re=170 pulsatile flow.

The time $t_{\max}$ required to reach the maximum integrated pixel intensity $A_{\max}$ describes the accumulation phase. Figure 9 also conveys that the maximum aggregate size is larger for smaller Re. This implies that during the accumulation phase, the difference between ferrofluid efflux due to downstream dispersion and influx through advective transport from the injection point decreases with increasing Re. In a manner similar to the accumulation phase, the dispersion time for an aggregate also decreases at higher Re, since washaway now occurs more rapidly due to the larger fluid shear. Therefore, the aggregate half-lives t_{half} are smaller at larger Re.

Transport of ferrofluid from the point of injection to where it is accumulated occurs mainly through advection (and to a small extent through diffusion). Therefore, we can ascribe a functional relationship between the rate of ferrofluid influx (to the aggregate) and the mean flow Re, i.e.,

$$\dot{M}_{\mathrm{in}}=f_1(\mathrm{Re}). \tag{1}$$

As already discussed in this paper, as well as in Ref. 21, ferrofluid washaway occurs from the periphery of the aggregate where the magnetic and shear forces are comparable. Intuitively, this rate would be a function of (i) the shear force, (ii) the size of the aggregate, and (iii) the magnetic force. Hence, we can represent the ferrofluid washaway rate as $\dot{M}_{\mathrm{out}}=f_2$ (Re, size, magnetic field). Since the projected area A of the aggregate is considered to be representative of

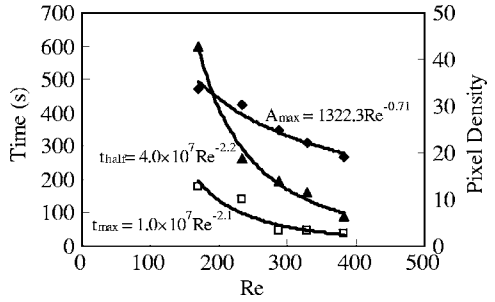

FIG. 10. Variation of the maximum pixel density (arbitrary unit) with Re for 3 μl of injected ferrofluid dispersing in a pulsatile flow at 1 Hz (α=12.5). Also the time to reach the maximum aggregate size (t_{max}) and the half-life (t_{half}) are plotted against Re. The mean variance of the curvefit relationships are 95.4%, 86.8%, and 97.7% for A_{max}, t_{max}, and t_{half}, respectively.

the aggregate size in this paper and the magnetic field distribution is held constant (as described in Fig. 2), the washaway rate

$$\dot{M}_{out} = f_3(\mathrm{Re}, A). \tag{2}$$

The growth rate of the aggregate is a function of $\dot{M}_{in}$ and $\dot{M}_{out}$, i.e., $dA/dt = f_4(\dot{M}_{in} - \dot{M}_{out})$. After integrating over time and using Eqs. (1) and (2), and denoting $\tilde{f}_4(\mathrm{Re}, A) = f_4[f_1(\mathrm{Re}) - f_3(\mathrm{Re}, A)]$,

$$A = \int_0^t \tilde{f}_4(\mathrm{Re}, A)\, dt, \tag{3a}$$

$$\text{or} \quad A = f_5(\mathrm{Re}, t). \tag{3b}$$

In the accumulation phase, $\dot{M}_{in} > \dot{M}_{out}$ and A grows over time. When $\dot{M}_{in} = \dot{M}_{out}$, the aggregate reaches its maximum size, i.e., $A_{max} = f_5(\mathrm{Re}, t_{max})$. Also, since $\dot{M}_{in} = \dot{M}_{out}$ at $t = t_{max}$, using Eqs. (1) and (2),

$$f_1(\mathrm{Re}) = f_2(\mathrm{Re}, A_{max}) \quad \text{or} \quad A_{max} = f_6(\mathrm{Re}). \tag{4}$$

Likewise,

$$t_{max} = f_7(\mathrm{Re}). \tag{5}$$

During the washaway phase $\dot{M}_{in} = 0$ and the aggregate size shrinks over time. Using Eq. (3b) to determine the expression for t_{half},

$$\frac{1}{2} A_{max} = f_5(\mathrm{Re}, t_{half}), \tag{6a}$$

$$\text{or} \quad t_{half} = f_8(\mathrm{Re}). \tag{6b}$$

Equations (4)–(6) indicate that, for a specified magnetic field distribution, A_{max}, t_{max}, and t_{half} can be represented as functions of Re. The functional relations f_6, f_7, and f_8 can be calculated provided f_1 and f_2 are known. Alternately, these parametric relationships are experimentally obtained when A_{max}, t_{max}, and t_{half} are plotted with respect to the mean Re, as shown in Fig. 10, yielding the relations $A_{max} \propto \mathrm{Re}^{-0.71}$, $t_{max} \propto \mathrm{Re}^{-2.1}$, and $t_{half} \propto \mathrm{Re}^{-2.2}$. The first of these indicates that the initial size of the ferrofluid aggregate mass varies inversely with the mean flow Re, i.e., the mass of the initial deposit decreases as Re increases. Both the accumulation phase duration t_{max} and the aggregate half-life t_{half} also have inverse dependence on Re through nearly identical relationships, differing only by a constant multiplier (i.e., $t_{half} \approx 4t_{max}$). The relations can be useful to design for the aggregation and dispersion of ferrofluids (e.g., during MDT or in ferrofluid-based pumps and valves), since they provide information about the ferrofluid aggregate lifetime at a target location. For instance, if MDT efficacy is to be expressed in terms of the aggregate size (that is representative of the total drug supply) and its half-life (that indicates the duration during which the drug is released at the target site), these relationships imply that the local blood flow Reynolds number is an important parameter.

IV. CONCLUSIONS

An experimental investigation of ferrofluid accumulation and dispersion under the influence of an imposed magnetic field is conducted in steady (for the purpose of comparison) and pulsatile flows. The response of ferrofluid aggregates to varying flow conditions is characterized.

1. Ferrofluid injected into the flow is transported downstream in the form of a streakline until the magnetic body force attracts the ferrofluid towards the region of strongest field gradient to form an aggregate where the Kelvin body force exceeds the fluid shear. A washaway region exists outside this core region, where the fluid shear is comparable to the magnetic body force, allowing for downstream ferrofluid dispersion. The aggregate first grows with time until the freshly injected supply ceases, after which it is depleted due to continuous washaway. In a Re=382 steady flow, ferrofluid washaway occurs in cycles at roughly 155 s intervals.
2. For a 1 Hz pulsatile flow with the same mean flow Re, the washaway time decreases fourfold and the aggregate centroid oscillates about a mean position with its downstream displacement being larger than upstream.
3. For a flow pulsation that has a primary 1 Hz component and a very weak 3 Hz component, the frequency spectrum of the ferrofluid aggregate shows peaks at these and other frequencies due to nonlinear interactions between the fluid shear and magnetic body force.
4. For the conditions investigated herein, the maximum aggregate size A_{max}, time to form this maximum size t_{max}, and the aggregate half-life t_{half} scale with the mean flow Re according to the relations $A_{max} \propto \mathrm{Re}^{-0.71}$, $t_{max} \propto \mathrm{Re}^{-2.1}$, and $t_{half} \propto \mathrm{Re}^{-2.2}$.

[1] S. Odenbach, "Recent progress in magnetic fluid research," J. Phys.: Condens. Matter **16**, R1135 (2004).
[2] R. E. Rosensweig, *Ferrohydrodynamics* (Cambridge University Press, Cambridge, 1985).
[3] Q. Chen and Z. J. Zhang, "Size-dependent superparamagnetic properties of $MgFe_2O_4$ spinel ferrite nanocrystallites," Appl. Phys. Lett. **73**, 3156 (1998).
[4] B. M. Berkovsky, "Some aspects of theoretical modeling of thermomechanics of magnetic fluids," in *Proceedings of the International Advanced Course and Workshop on Thermomechanics of Magnetic Fluids*, edited by B. M. Berkovsky (Hemisphere, Washington, D.C., 1978), pp. 149–157.

[5]G. K. Kouassi, J. Irudayaraj, and G. McCarty, "Activity of glucose oxidase functionalized onto magnetic nanoparticles," Biomag. Research Technol.1477-044X **3**, 1 (2005).
[6]R. E. Goldstein, D. P. Jackson, and S. A. Langer, "Dynamics of pattern-formation in magnetic fluids," J. Magn. Magn. Mater. **122**, 267 (1993).
[7]I. J. Jang, H. E. Horng, Y. C. Chiou, C-Y. Hong, J. M. Yu, and H. C. Yang, "Pattern formation in microdrops of magnetic fluids," J. Magn. Magn. Mater. **201**, 317 (1999).
[8]A. Sinha, R. Ganguly, and I. K. Puri, "Magnetically assembled 3-d mesoscopic patterns using a suspension of superparamagnetic nanoparticles," *ASME Integrated Nanosystems-Design, Synthesis and Applications*, Pasadena, CA, September 2004, Paper No. NANO2004–46091.
[9]H. Hartshorne, C. J. Backhouse, and W. E. Lee, "Ferrofluid-based microchip pump and valve," Sens. Actuators B **99**, 592 (2004).
[10]K. Mosbach and U. Schröder, "Preparation and application of magnetic polymers for targeting of drugs," FEBS Lett. **102**, 112 (1979).
[11]A. S. Lubbe, C. Alexiou, and C. Bergemann, "Clinical applications of magnetic drug targeting," J. Surg. Res. **95**, 200 (2001).
[12]A. Jordan, R. Scholz, K. Maier-Hauff, M. Johannsen, P. Wust, J. Nadobny, H. Schirra, H. Schmidt, S. Deger, S. Loening, W. Lanksch, and R. Felix, "Presentation of a new magnetic field therapy system for the treatment of human solid tumors with magnetic fluid hyperthermia," J. Magn. Magn. Mater. **289**, 331 (2001).
[13]Q. A. Pankhurst, J. Connolly, S. K. Jones, and J. Dobson, "Applications of magnetic nanoparticles in biomedicine," J. Phys. D **36**, R167 (2003).
[14]G. T. Gillies, R. C. Ritter, W. C. Broaddus, M. S. Grady, M. A. Howard III, and R. G. McNeil, "Magnetic manipulation instrumentation for medical physics research," Rev. Sci. Instrum. **65**, 533 (1994).
[15]G. I. Taylor, "Dispersion of soluble matter in solvent flowing slowly through a tube," Proc. R. Soc. London, Ser. A **219**, 186 (1953).
[16]R. Smith, "Contaminant dispersion in an oscillatory flow," J. Fluid Mech. **114**, 379 (1982).
[17]P. A. Voltairas, D. I. Fotiades, and L. K. Michalis, "Hydrodynamics of magnetic drug targeting," J. Biomech. **35**, 813 (2002).
[18]E. K. Ruuge and A. N. Rusetski, "Magnetic fluids as drug carriers: targeted transport of drugs by a magnetic field," J. Magn. Magn. Mater. **122**, 335 (1993).
[19]C.-Y. Chen and C.-Y. Liao, "Motion of miscible magnetic fluids in a dynamic magnetic field," Int. J. Numer. Methods Heat Fluid Flow **13**, 244 (2003).
[20]R. Ganguly, A. P. Gaind, S. Sen, and I. K. Puri, "Characterizing ferrofluid transport for magnetic drug targeting," J. Magn. Magn. Mater. **289**, 331 (2005).
[21]R. Ganguly, A. P. Gaind, and I. K. Puri, "A strategy for the assembly of three-dimensional mesoscopic structures using a ferrofluid," Phys. Fluids **17**, 057103 (2005).
[22]E. Blūms, J. Pļaviņš, and A. Chukhrov, "High-gradient magnetic separation of magnetic colloids and suspensions," J. Magn. Magn. Mater. **39**, 147 (1983).
[23]M. Zahn, *Electromagnetic Field Theory* (Wiley, New York, 1979).
[24]K. B. Chandran, *Cardiovascular Biomechanics* (New York University Press, New York, 1992).